Hindawi Publishing Corporation
Journal of Nanotechnology
Volume 2011, Article ID 569036, 6 pages
doi:10.1155/2011/569036

Research Article

Synthesis and Humidity Sensing Properties of Sn-Doped Nano-TiO_2

P. Raji,[1] H. S. Binitha,[2] and K. Balachandra Kumar[3]

[1] *Department of Physics, Mepco Schlenk Engineering College, Sivakasi 626 005, Tamilnadu, India*
[2] *Department of NanoScience and Technology, Mepco Schlenk Engineering College, Sivakasi 626 005, Tamilnadu, India*
[3] *Department of Physics, Kamaraj College of Engineering and Technology, Virudhunagar 626 001, Tamilnadu, India*

Correspondence should be addressed to P. Raji, rajimku@rediffmail.com

Received 9 March 2011; Accepted 21 June 2011

Academic Editor: John A. Capobianco

Nanostructured Sn-doped TiO_2 have been prepared by ball milling using SnO_2 and TiO_2 as raw materials. The as-prepared powders are characterized by XRD, SEMs and EDAX to identify the structural phases, surface morphology, and composition of the materials. The materials are prepared with the addition of tin of different molar ratios (0, 0.05, 0.10, 0.15, 0.20, 0.25, and 1.0) to TiO_2 and sintered at 800°C for 3 h. They are subjected to dc resistance measurements as a function of relative humidity (RH) in the range of 30%–97% in a self-designed humidity chamber, and the results revealed that the sensitivity factor increased with an increase in tin molar ratio. Among them, TiO_2—20 wt% of SnO_2 possessed the highest humidity sensitivity, while the pure TiO_2 and SnO_2 composite possessed a low sensitivity.

1. Introduction

The development of humidity sensors has received much attention during the last years due to the necessity of controlling and monitoring environments in many different fields like industrial processes and domestic comfort [1–3]. Since each application field requests distinct operating conditions and generally sensor elements work in narrow ranges of humidity and temperature, the selection of a material should be based on certain conditions, in order to assure the satisfactory operation of the humidity sensor, that include good sensitivity, linearity over the range of application, fast response, low hysteresis, and stability in the exhibition to impurities present in the environment [3–6].

As a consequence, a wide variety of materials have been researched with the objective to study their sensitivity, usually variations of electrical parameters in relation to the humidity in the atmosphere. These materials are based on polymers, electrolytes, and especially ceramics [1, 3].

At present, ceramic materials possess a certain prominence due to their properties, which exhibit advantages regarding their mechanical resistance, and physical and chemical stability. The humidity-sensitivity properties of a ceramic are mostly influenced through the porous microstructure and the surface reactivity with moisture. Porous ceramic materials based on metals oxides have been largely used as humidity sensors [2]. The principle of humidity measurement with ceramic sensors is the change in electrical capacitance and conductance owing to water vapor chemisorption and physisorption and/or capillary condensation in the pores of the ceramic sensor.

TiO_2-based humidity sensors are studied vigorously, as it is likely to show better sensitivity because of its hydrophilic property [7]. It is studied more in thin film form [8]. However, it is reported that thin film sensors show lower sensitivity than those shown by porous ceramic sintered counterparts [7–9]. TiO_2 is known to have a hysteresis in humidity sensitivity curve. It was thought that the use of additives would be useful to get over this drawback. The additives are reported to minimize the hysteresis in TiO_2 humidity sensors [10]. Additives are also reported to improve performance parameters of TiO_2 humidity sensors [11–15]. SnO_2 is known as isostructural to a rutile phase of TiO_2, and fairly good electrical conductor was considered preferentially as an additive. Although thin films have many advantageous properties for sensor applications, achieving porous thin

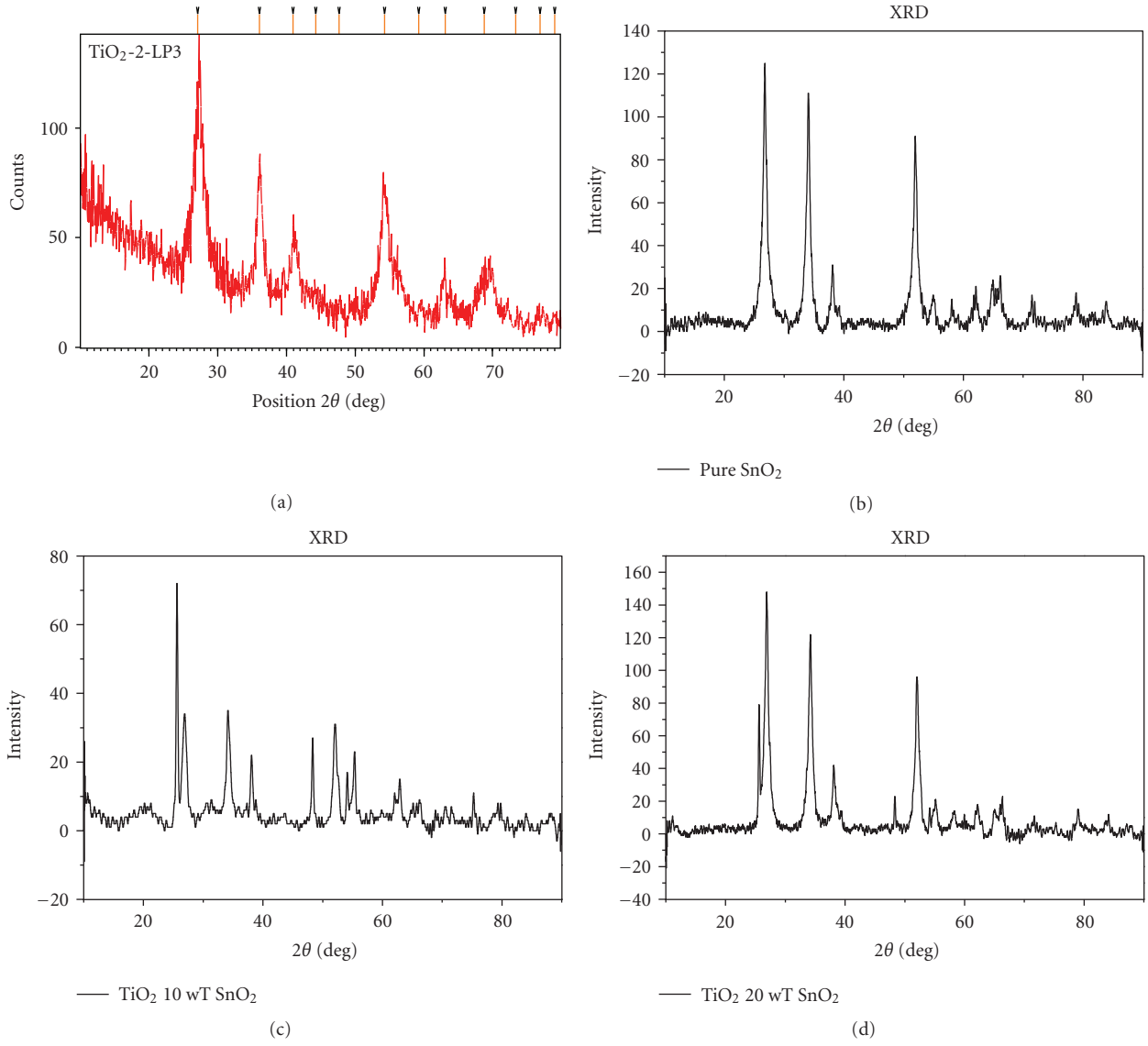

FIGURE 1: (a) TiO_2, (b) SnO_2, (c) $Ti_{0.90}Sn_{0.10}O_2$, and (d) $Ti_{0.75}Sn_{0.25}O_2$.

films by use of energy intensive thin film formation processes has remained an unsolved problem for the scientists.

The aim of this work is to synthesize and investigate humidity sensing properties of Sn-doped nano-TiO_2 ceramic material by ball milling.

2. Experimental

To synthesize Sn-doped nano-TiO_2, raw materials 99.5% pure TiO_2 (Aldrich) and 98% pure SnO_2 (Aldrich) are used. We have prepared pure TiO_2, SnO_2, and $Ti_{1-x}Sn_xO_2$ composition, where x = 5, 10, 15, 20, 25 wt% of SnO_2. A planetary ball mill (Fritsch Company) was used with its vial rotation of 300 rpm. The vial and balls are made of steel. The raw materials are milled for 5 hours. The total mass of powder was about 50 gm and the ratio of balls to powder is 1 : 1. Milling was interrupted for 15 minutes to suppress the excessive temperature rise of the vial and balls. Now, pellets of these materials were made using a hydraulic pressing machine under the pressure of 55158 KPascal at room temperature. Size of each pellet was 5 cm diameter and 4 mm thickness. Each pellet was annealed at 800°C for 3 hours inside an electric furnace. Each pellet was kept within an electrode holder and has been exposed to humidity in the self-designed humidity chamber, and variations in resistance with humidity have been recorded. Relative humidity is measured using standard hygrometer. Variations in resistance were noted by using sinometer.

3. Characterization

3.1. XRD. A well-crystallized anatase form has been found for undoped TiO_2 (Figure 1(a), which corresponds well with the JCPDS data file no. 21-1272. With 0.05%, 0.10%,

and 0.15% of Sn, a mixture of anatase and rutile phases has been observed with rutile being the predominant one. Figure 1(c) suggests that the presence of Sn retards the anatase grain growth and accelerates anatase to rutile phase transformation. As Figure 1(d) shows, for 0.20% of Sn, a completely rutile solid solution is formed with no traces of anatase TiO_2. All the peaks observed for this sample correspond to JCPDS data for rutile TiO_2 (File no. 1276). Also, no peak for either metallic Sn or SnO_2 could be observed even with 0.25 at% of Sn (Figure 1(d)). These results indicate that there is complete solubility of Sn in rutile TiO_2 in the studied composition range and for about 0.20 at % of Sn and anatase TiO_2 is completely transformed into the rutile form with a nominal composition of $Sn_{0.20}Ti_{0.80}O_2$. The ionic radii being comparable ($r_{Sn^{2+}}$ 83 pm and $r_{Ti^{4+}}$ 74 : 5 pm in octahedral coordination), Sn^{2+} ions can easily enter the TiO_2 lattice to form a stable solid solution. Figure 1(b) show that the XRD spectra of the pure SnO_2 show reflection from the (110), (101), (200), (220), and (310) and XRD pattern matched well with the rutile phase of SnO2. (JCPDS file no. 44-0872).

Apart from forming solid solution with TiO_2, addition of SnO_2 also affects the crystallite size and particle size of the composition. Table 1 summarizes the observations of structural properties of Sn-doped TiO_2- and the particle size was evaluated from XRD by employing the Scherrer equation ($d = 0.9\lambda/2\beta\cos\theta$). An important observation is that the surface area increases and particle size decreases with increasing concentration of SnO_2.

3.2. EDAX. Figure 2 shows the EDAX spectrum of 20 wt% TiO_2-SnO_2 nanopowder. The peak indicates that no elements other than Sn, O, and Ti were detected. The Au C peak originates from the gold sputtered sample from SEM measurement. The atomic percent of tin to titanium was determined as 80 : 20, which is good in agreement with the expected value. From this spectrum, it is found that strong signals from the tin, titanium, and oxygen atoms in the nanoparticles.

3.3. SEM. In Figure 3 the SEM image reveals that they possess the grain size of nanometer order and have nanoporous structure. It means that the structure is likely to facilitate the adsorption process of water molecules because of the capillary pore and large surface area.

4. Device Assembly

4.1. Fabrication Procedure. Device assembly has been shown in Figure 4. A glass box is designed of dimensions, length 42 cm, breadth 21 cm, and height 27.5 cm with a suitable door at one side. The door is used to place the sample inside the chamber and to analyze the humidity sensing property. This arrangement was helpful to increase the humidity inside the chamber. Inside the glass box, there are two stands, one for placing the solution which varies the relative humidity and the other for placing the sample which is in the pellet form.

Table 1: Lattice constants of Sn-doped TiO_2.

$Ti_{1-x}Sn_xO_2$	a (Å)	(Å)	Particle size (SEM)	Particle size (XRD)
$x = 0$	3.7685	9.4690	45	28
$x = .10$	3.773	9.4974	40	20
$x = .20$	3.7642	9.459	33	14
$x = 1$	4.7331	3.1842	50	21

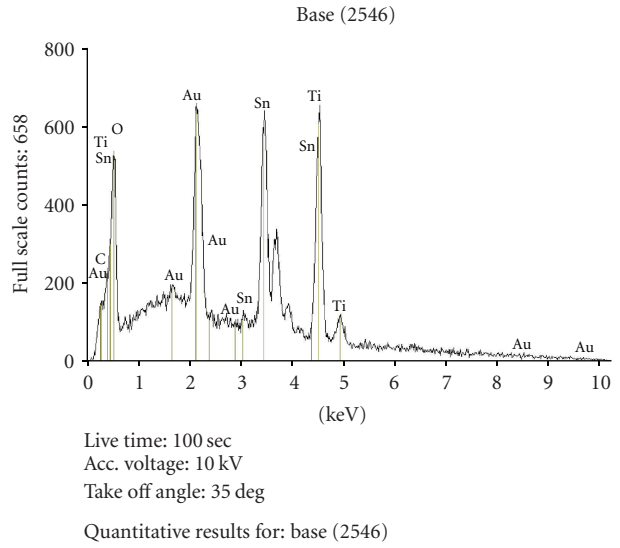

Figure 2: EDAX for $Ti_{0.80}Sn_{0.20}O_2$.

The Cu-pellet-Cu electrode arrangement is fixed on a nonconducting base inside the glass box such that connecting wires remain outside the chamber. Saturated aqueous solution of potassium sulphate in a small container has been placed inside the glass box, and it increases the humidity inside box. The percentage relative humidity (RH %) inside the box is increased from 33.1% to 97.6%. Relative humidity in % is measured by using hygrometer. Variations in the resistance have been noted by using sinometer of MΩ order. All the measurements are carried out at room temperature. After each change of the humidity, the sensor element was exposed to the new humidity for 2 minutes before measuring the new resistance. Relative humidities ranging from 33.1% to 97.6% were obtained using saturated solutions as the humidity generation source. A list of saturated salts and their constant humidity values is given in Table 2.

To examine stability of the sensors, the humidity-resistivity characteristics at room temperature, between 33% to 97.6% RH, were measured after 5 days, and no important changes were observed. In fact, the sensor resistance slightly increased in room temperature after aging.

Humidity response was defined as the ratio of the resistance change occurred in a sample under exposure of the humidity to the original resistance

$$S = \frac{R_0 - R_H}{R_0} = \frac{\Delta R}{R_0}, \quad (1)$$

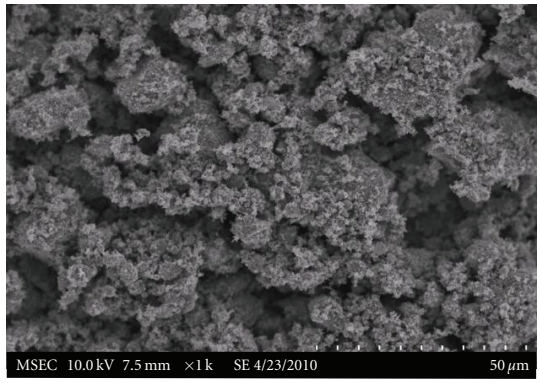

(a)

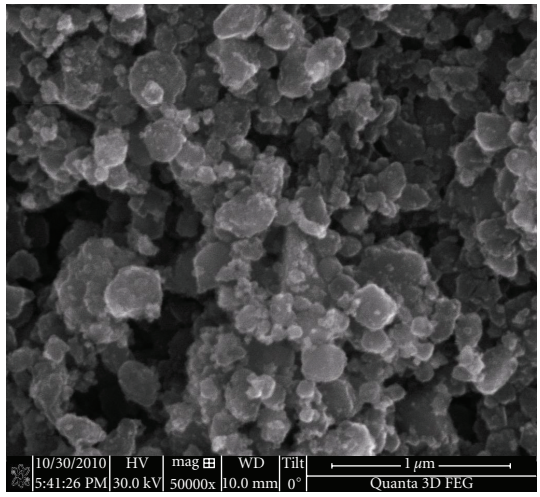

(b)

Figure 3: (a) TiO_2, and (b) $Sn_{.10}Ti_{.90}O_2$.

where R_0 is the resistance in dry air and R_H is the resistance in relative humidity. Response time is calculated by the time required for the sensor to attain the maximum change in resistance. The recovery time is also predicted by the time taken to get back their original resistance.

4.2. Humidity Sensing Properties Studies. Figures 5(a)–5(c) show the variation of resistance as a function of the relative humidity for the pure TiO_2, pure SnO_2, and $Ti_{0.80}Sn_{0.20}O_2$ at room temperature. As the RH increases, the resistance decreases by three orders in RH range 30, to 97%. The change is linear for the all composites except for pure SnO_2, suggesting that mechanism of resistance variation is similar over the region of 30%–97%. However, in case of SnO_2, the resistance (R) versus RH plot is clearly nonlinear for the RH > 60%. The nonlinearity of SnO_2 sample might be due to the inhomogenous absorption of water molecule.

5. Results and Discussions

For the pure TiO_2, pure SnO_2 and various composition of SnO_2 (5 wt%, 10 wt%, 15 wt%, 20 wt%, and 25 wt%), there will be a large decrease in resistance with increased relative humidity. It is due to the adsorption of water vapours on the surface with large surface area and capillary pores. The water vapors are adsorbed on the grain surface and in the pores. The nanoscaled grains lead to much more grain boundaries and nanopores, leading to more active sites available for condensed water to react. The high surface area provides more sites for water adsorption and produces more charge carriers for electrical conduction.

The conduction behavior of TiO_2-SnO_2 in the presence of water vapor is mainly due to ions. In this sensing material, Sn_{4+} cations are assumed to be highly active site for adsorption because of its highest charge density. These ions readily combines with hydroxyl group of adsorbed water and weaken the bond between hydroxyl ions and protons, and subsequently, water molecules gets dissociated. This provides free protons for electrical conduction. The hydroxyl ions thus remain chemically adsorbed at the cationic sites. Therefore, the first layer of adsorbed water molecule forms a chemisorbed layer and this process is irreversible at room temperature. The subsequent layers are physically adsorbed on the first layer to form hydroxyl multilayers by hydrogen bonding. These free mobile protons obtained from the first chemisorbed layer react with physisorbed water layer and form hydronium ions.

When physically adsorbed layer is abundant, the protons from one hydronium ion can hop to another hydronium ion, this proton transfer mechanism provides the mean for electrical conduction. The physisorption of water layer is reversible at room temperature, and it exists in equilibrium with ambient humidity. As the ambient humidity varies, the amount of water vapour physisorbed on the surface or condensed on the capillary pores varies, subsequently changing the concentration of the mobile protons, which in turn changes the conductivity of the ceramic.

6. Conclusions

Sn-doped nano-TiO_2 was investigated for its humidity sensing characteristics. The sensing material annealed at 800°C gave nanocrystals of average size 20–50 nm which had good sensing properties for water vapour. Although the doping of Sn_{4+} increases the surface area of powders, responsible for humidity sensitivity, the segregation of Sn_{4+} at grain boundaries would be unfavorable factor as hydrophilicity of TiO_2 would decrease. This is reflected in the study of various compositions in our study. $x = 0.1$ gives better results with respect to sensitivity and minimum hysteresis than $x = 0.2, 0.3$ although these compositions are superior to the $x = 0.1$ composition in terms of lower particle size and hence higher surface area.

This sensing element shows the maximum average sensitivity 7.5. Nearly all the sensing elements have shown similar trend that is at minimum RH% the resistance is maximum, and at maximum RH% the resistance is minimum. This study has significance in viewing of variations in properties of TiO_2 after addition of tin oxide. The humidity sensor reported in this paper is easy to fabricate, cheap, friendly for users, and sensitive to the entire range of RH. This is applicable to commercial production.

Table 2: Relative humidity above saturated salt solutions.

Salt	$MgCl_2$	K_2CO_3	$Mg(NO_3)_2$	$CoCl_2$	NaCl	KCl	K_2SO_4
Relative humidity (%)	33.1	43.2	53.0	64.0	75.7	85.1	97.6

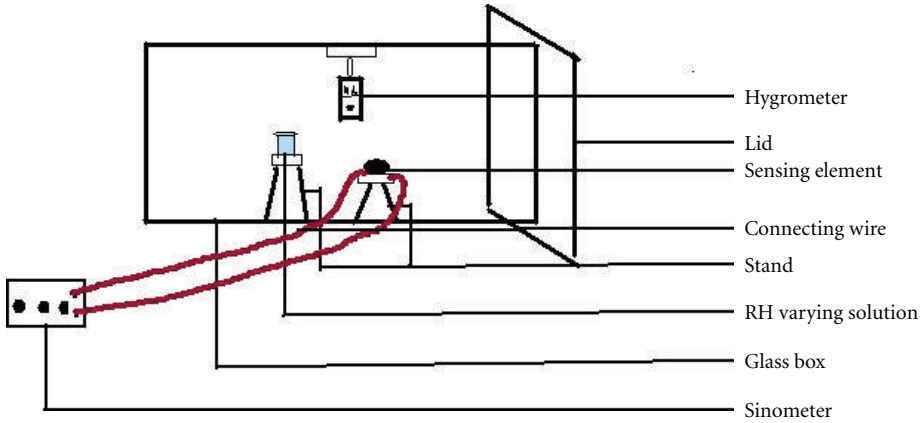

Figure 4: A Schematic diagram of device assembly.

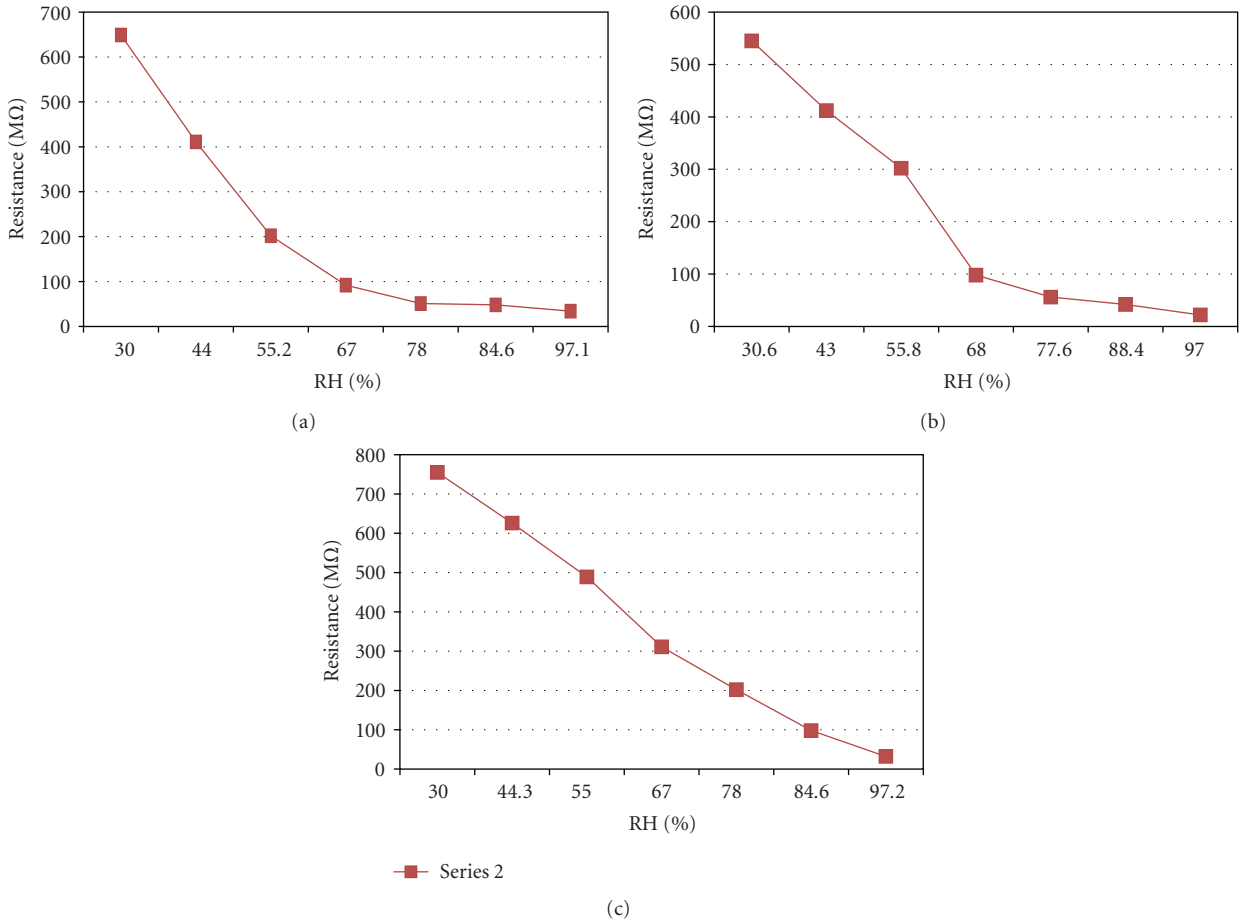

Figure 5: (a) TiO_2, (b) SnO_2, and (c) $Ti_{0.80}Sn_{0.20}O_2$.

References

[1] J. G. Fagan and V. R. W. Amarakoon, "Reliability and reproducibility of ceramic sensors: part ffl, humidity sensors," *Bulletin of the American Ceramic Society*, vol. 72, p. 119, 1993.

[2] B. M. Kulwicki, "Humidity sensors," *Journal of the American Ceramic Society*, vol. 74, no. 4, pp. 697–707, 1991.

[3] E. Traversa, "Ceramic sensors for humidity detection: the state-of-the-art and future developments," *Sensors and Actuators: B*, vol. 23, pp. 135–156, 1995.

[4] M. Greenblatt and P. Shuk, "Solid-state humidity sensors," *Solid State Ionics*, vol. 86–88, no. 2, pp. 995–1000, 1996.

[5] I. S. Mulla, V. A. Chaudhary, and K. Vijayamohanan, "Humidity sensing properties of boron phosphate," *Sensors and Actuators: A*, vol. 69, no. 1, pp. 72–76, 1998.

[6] G. Fu, H. Chen, Z. Chen, J. Zhang, and H. Kohler, "Humidity sensitive characteristics of Zn_2SnO_4-$LiZnVO_4$ thick films prepared by the sol-gel method," *Sensors and Actuators: B*, vol. 81, no. 2-3, pp. 308–312, 2002.

[7] J. Slunecko and M. Hrovat, "Temperature characteristics of electrical properties of $(Ba,Sr)TiO_3$ thick film humidity sensors," *Sensors and Actuators: B*, vol. 26-27, pp. 99–102, 1995.

[8] M. Fukazawa, H. Matuzaki, and K. Hara, "Humidity- and gas-sensing properties with an Fe_2O_3 film sputtered on a porous Al_2O_3 film," *Sensors and Actuators: B*, vol. 14, pp. 521–522, 1993.

[9] A. Bearzotti, A. Bianco, and E. Traversa, "Humidity sensitivity of sputtered TiO_2 thin films," *Sensors and Actuators: B*, vol. 18-19, pp. 525–528, 1994.

[10] W. P. Tai, J. G. Kim, and J. H. Oh, "Humidity sensitive properties of nanostructured Al-doped $ZnO:TiO_2$ thin films," *Sensors and Actuators: B*, vol. 96, pp. 477–481, 2003.

[11] F. Uchikawa and K. Shimamoto, "Time variability of surface ionic conduction on humidity-sensitive SiO_2 films," *The American Ceramic Society Bulletin*, vol. 64, no. 8, pp. 1137–1141, 1985.

[12] Y. Sadaoka, Y. Sakai, and S. Mitsui, "Humidity sensor using zirconium phosphates and silicates. Improvements of humidity sensitivity," *Sensors and Actuators*, vol. 13, no. 2, pp. 147–157, 1988.

[13] Y. Ichinose and S. Tanaka, "Preparation and humidity-sensitive characteristics of fluorapatite compounds," *Sensors Mater*, vol. 1, pp. 77–81, 1988.

[14] T. Y. Kim, D. H. Leea, Y. C. Shima, J. U. Bua, and S. T. Kim, "Effects of alkaline oxide additives on the microstructure and humidity sensitivity of $MgCr_2O_4$—TiO_2," *Sensors and Actuators: B*, vol. 9, no. 3, pp. 221–225, 1992.

[15] G. Montesperelli, A. Pumo, E. Traversa et al., "Sol-gel processed TiO_2-based thin films as innovative humidity sensors," *Sensors and Actuators: B*, vol. 24-25, pp. 705–709, 1995.